scientific reports

Check for updates

OPEN

# Effect of preparation methods of $CeO_2$ on the properties and performance of Ni/$CeO_2$ in $CO_2$ reforming of $CH_4$

Zenan Ni✉, Xavier Djitcheu, Xiaoxu Gao, Jian Wang, Huimin Liu✉ & Qijian Zhang

**$CO_2$ reforming of $CH_4$ (CRM) is not only beneficial to environmental protection, but also valuable for industrial application. Different $CeO_2$ supports were prepared to investigate the matching between Ni and $CeO_2$ over Ni/$CeO_2$ and its effect on CRM. The physicochemical properties of Ni/$CeO_2$-C (commercial $CeO_2$), Ni/$CeO_2$-H (hydrothermal method) as well as Ni/$CeO_2$-P (precipitation method) were characterized by XRD, $N_2$ adsorption at − 196 °C, TEM, SEM–EDS, $H_2$-TPR, $NH_3$-TPD and XPS. $Ni^0$ with good dispersion and $CeO_2$ with more oxygen vacancies were obtained on Ni/$CeO_2$-H, proving the influence on Ni/$CeO_2$ catalysts caused by the preparation methods of $CeO_2$. The initial conversion of both $CO_2$ and $CH_4$ of Ni/$CeO_2$-H was more than five times that of Ni/$CeO_2$-P and Ni/$CeO_2$-C. The better matching between Ni and $CeO_2$ on Ni/$CeO_2$-H was the reason for its best catalytic performance in comparison with the Ni/$CeO_2$-C and Ni/$CeO_2$-P samples.**

With the technology breakthrough in exploiting shale gas and combustible ice, searching clean approaches to utilize the main component $CH_4$ efficiently has received extensive attention[1,2]. $CO_2$ reforming of $CH_4$, generally short for CRM, could convert greenhouse gas $CH_4$ and $CO_2$ to syngas ($CO + H_2$). CRM is of great practical significance due to the following advantages: (1) the $n(H_2)/n(CO)$ ratio of the produced syngas is about 1, which could be directly used for Fischer–Tropsch synthesis; (2) $CO_2$ and $CH_4$ are greenhouse gases, and the utilization of them could really improve the ecological environment; (3) CRM requires high heat input, which means CRM could be employed for energy storage and transmission medium[3,4].

Noble metal catalysts, such as Rh-[5], Ru-[6], Pd-[7] based catalysts, exhibited good catalytic activity and strong anti-coking capacity in CRM. However, they could not be applied on an industrial scale because of their limited resources. On the contrary, the cheap and abundant non-noble metal catalysts, especially Ni-based catalysts, which give catalytic activities comparable to that of noble metal-based catalysts, have been widely studied[8–10]. Unfortunately, Ni-based catalysts generally suffer from poor stability. On one hand, at the high operating temperature of endothermic CRM (700–850 °C), Ni particles aggregate easily, which may reduce the number of active sites of the catalysts and eventually weaken the catalytic capacity[11]. On the other hand, filamentous carbon and active carbon are produced via $CH_4$ cracking and CO disproportionation reactions. The accumulation and growth of these carbon species gradually cover and embed the active Ni particles and ultimately result in deteriorated catalyst stability[12,13]. Therefore, designing efficient Ni-based catalysts with strong anti-aggregation and anti-coking competence is critical for improving their stability in CRM.

With the aim to improve the anti-agglomeration competence of Ni-based catalysts, several approaches have been adopted, including (1) adding a structure promoter to stabilize Ni particles and (2) enhancing the Ni-support interaction to prevent the movement of Ni particles. For example, the Ni particles on Ni/SBA-15 catalyst modified by 1 wt% Sn (served as the structure promoter) were smaller and not easy to aggregate than those on unmodified catalyst[14]; the strong interaction between Ni and $Al_2O_3$ over Ni/$Al_2O_3$ catalyst, evidenced by the formation of $NiAl_2O_4$, prevents the aggregation of Ni particles greatly[15,16]. As for improving the anti-coking competence of Ni-based catalysts, the following routes are proved promising. (1) Adopting Ni-based catalysts with small Ni particles, since it is well accepted that smaller Ni particles exhibit stronger anti-coking competence[17,18]; (2) Adjusting the basic properties of Ni-based catalysts to facilitate $CO_2$ adsorption and accelerate reverse CO disproportionation reaction, which could help to eliminate the deposited coke by the adsorbed $CO_2$[19,20]. (3)

School of Chemical and Environmental Engineering, Liaoning University of Technology, Jinzhou 121001, China. ✉email: hgnzn@lnut.edu.cn; liuhuimin08@tsinghua.org.cn

Utilizing a material with strong oxygen storage capacity as support, which could serve as an oxygen reservoir for the elimination of deposited coke via oxidation reaction[21,22].

Based on the research progress made by predecessors, it could be speculated that $Ni/CeO_2$ catalyst with a large specific surface might be good for CRM, owing to (1) the Ni particles on a catalyst with a large specific surface area are generally well dispersed, and the interaction between Ni particles and $CeO_2$ might be strong; (2) $CeO_2$ is of basic properties[23], which could facilitate $CO_2$ adsorption and help to eliminate the deposited coke; (3) the oxidation–reduction property of $CeO_2$ renders it as a strong oxygen reservoir[24], which is ready to react with the deposited coke. Several groups have synthesized $Ni/CeO_2$ catalysts and investigated their performance in CRM. However, controversial conclusions have been obtained. For instance, Shao et al. synthesized $Ni/CeO_2$ via microemulsion method and reported that the as-prepared catalyst had smaller Ni particles (6–13 nm, with an average of 11 nm) and exhibited high activity in CRM[25]. Yahi et al. compared the catalytic performance of $Ni/CeO_2$ prepared by auto-combustion method, sol–gel method and microemulsion method. It is discovered that, $Ni/CeO_2$ prepared by microemulsion method (the average size of Ni particles were 11 nm) did not show any catalytic activity[26]. Holgado et al. got $Ni/CeO_2$ (the size of Ni particles was in the range of 12–18 nm) by combustion method, which recorded a high activity but poor stability[27]. Rosen et al. synthesized $Ni/CeO_2$ solid solution via exsolution method, which showed active and stable performance in CRM at 800 °C (The size of Ni particles was not clearly stated)[28]. Rodriguez et al. utilized theoretical calculation to investigate $Ni/CeO_2$ catalyst and reported that it was a highly active catalyst for CRM even at a temperature as low as 700 K, and the strong interaction between Ni and $CeO_2$ plays crucial roles in cleaving the C–H bond in $CH_4$[29]. Ganduglia-Pirovano et al. considered that $Ce^{3+}$ sites and the interaction between Ni and $CeO_2$ worked in concert to cleave the C–H bond[30]. Zhu et al. treated Ni and $CeO_2$ by plasma to get clean Ni–$CeO_2$ interface, which was regarded to be responsible for its high activity in CRM[31]. Therefore, the preparation method of $CeO_2$ has a great influence on the activity of $Ni/CeO_2$ in CRM. Many studies focus on the small size of Ni, however, sometimes, $Ni/CeO_2$ catalysts with small size of Ni still exhibit unsatisfactory catalytic performance. The controversial conclusions might be caused by the poor matching between Ni and $CeO_2$ supports, and it is difficult to get a generalized guidance for the rational design of efficient catalysts.

For studying the impact of the synthesis procedures of $CeO_2$ supports on the catalytic performance of the binary oxides, the low Ni content and the introduction method of Ni were control the same, and $CeO_2$ prepared by three different methods were used as the supports of $Ni/CeO_2$ catalysts. The properties of three kinds of $CeO_2$ and their supported Ni-based catalysts were characterized, and the performance of $Ni/CeO_2$ catalysts in CRM were evaluated.

## Experimental section

**Catalyst preparation.** Chemicals in this study were of analytical grade and used as received. $CeO_2$-H was used to denote $CeO_2$ prepared by hydrothermal method. It was prepared via the following procedure: 11.2 g $CeCl_3{\cdot}7H_2O$ and 9.4 g cetyltriethylammnonium bromide (CTAB) were firstly dissolved in 550 mL deionized water, to which 25 mL 25 wt% $NH_3$ solution was then added drop-wisely. The slurry was stirred at room temperature for 1 h and then treated at 90 °C for 30 h with reflux. After cooling down to room temperature, it was washed by deionized water and acetone to neutral. Finally, it was dried at 80 °C for 24 h and calcined in air at 700 °C (at a heating ramp of 2 °C $min^{-1}$) for 5 h to obtain $CeO_2$-H. $CeO_2$-P was used to denote $CeO_2$ prepared by precipitation method. It was prepared via the following procedure: 250 mL 0.2 wt% $NH_3$ solution and 250 mL 16.0 g $L^{-1}$ $CeCl_3$ solution were added drop-wisely to another 250 mL 0.2 wt% $NH_3$ solution under vigorous stir. The slurry was stirred at room temperature for 1 h and then aged for 12 h. After centrifugation, it was washed by deionized water and acetone to neutral. Finally, it was dried at 80 °C for 24 h and calcined in air at 700 °C (at a heating ramp of 2 °C $min^{-1}$) for 5 h to obtain $CeO_2$-P.

$CeO_2$-H, $CeO_2$-P, together with commercial $CeO_2$ (denoted as $CeO_2$-C) were used as supports of Ni-based catalysts. $Ni/CeO_2$ catalysts were prepared by loading a certain amount of $Ni(NO_3)_2$ onto the $CeO_2$ supports using the wetness impregnation method. After impregnating for 10 h, the samples were evaporated, dried at 80 °C and calcined at 700 °C for 5 h. The as-prepared catalysts were denoted as $Ni/CeO_2$-H, $Ni/CeO_2$-P and $Ni/CeO_2$-C, respectively.

**Catalyst characterization.** The crystalline structures of $CeO_2$ and $Ni/CeO_2$ catalysts were determined by X-ray diffraction (XRD) method on an X-Pert diffractometer equipped with graphite monochromatized Cu-Kα radiation. The specific surface areas were determined using a surface area analyzer (BEL Sorp-II mini, BEL Japan Co., Japan) with the Brunauer–Emmett–Teller (BET) method. Shape of the samples were observed using a transmission electron microscope (TEM-16-TS-008) and scanning electron microscopy (SEM) equipped with energy-dispersive X-ray spectroscopy (EDS). $H_2$-temperature programmed reduction (TPR), $CO_2$-temperature programmed desorption ($CO_2$-TPD) and $NH_3$-temperature programmed desorption ($NH_3$-TPD) profiles were carried out over Quantachrome instrument, with the temperature raising from room temperature to 900 °C at a heating rate of 10 °C $min^{-1}$. X-ray photoelectron spectroscopy (XPS) was carried out on Thermo Fisher equipped with Al Kα radiation. Binding energies were calibrated by carbon (C 1*s*, 284.6 eV). The amount of coke deposited on the spent catalysts was characterized by Thermogravimetry (TG). The composition of the samples was determined by inductively coupled plasma-optical emission spectrometry (ICP-OES) on a 730 Series ICP-OES by Agilent Technologies.

**Catalyst evaluation.** CRM reaction was conducted in a fixed-bed reactor under atmospheric pressure. A portion of 0.20 g catalyst was packed uniformly in the temperature-constant zone of a quartz tube. Before reaction, the catalysts were reduced by 20% $H_2$/Ar at 700 °C for 1 h. Then 20.0 mL $min^{-1}$ (STP) $CH_4$ and 20.0

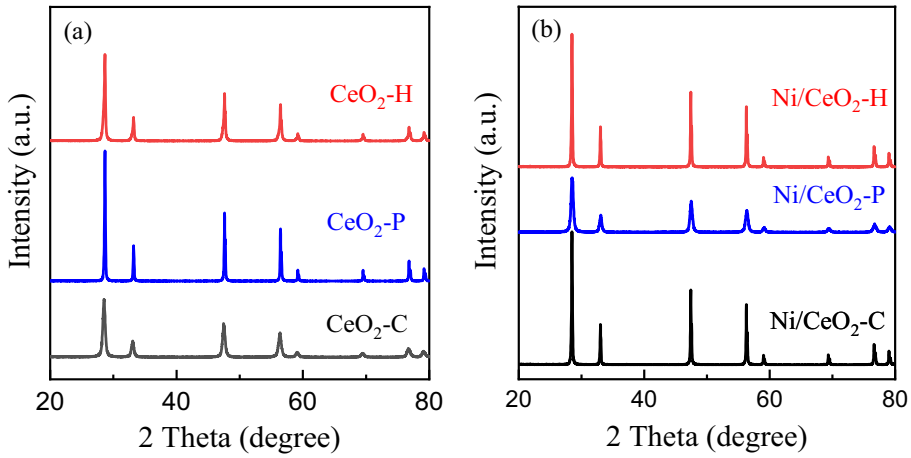


**Figure 1.** XRD patterns of (**a**) $CeO_2$ supports and (**b**) Ni/$CeO_2$ catalysts.

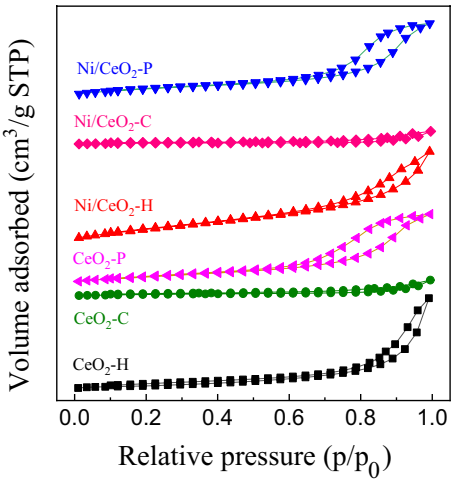


**Figure 2.** $N_2$ adsorption–desorption isotherms of $CeO_2$ based catalysts.

mL $min^{-1}$ (STP) $CO_2$ were introduced into the reactor as reactants, with WHSV of 4.3 $h^{-1}$ for $CH_4$ and 11.8 $h^{-1}$ for $CO_2$. After removing the byproduct water via an ice trap, the effluent gas was analyzed by a gas chromatography equipped with a TDX-01 column to determine the relative amounts of $CH_4$, CO, $CO_2$ and $H_2$, and the flow rate of the effluent gas was measured with a flow meter.

## Results and discussion

**Crystalline structure of $CeO_2$ and Ni/$CeO_2$ catalysts.** The crystalline structures of $CeO_2$ and Ni/$CeO_2$ catalysts were characterized by XRD, and the results were displayed in Fig. 1. The intense and sharp diffraction peaks at 28.6, 33.1, 47.5, 56.3, 59.1, 69.4, 77.0 and 79.1 in Fig. 1a were assigned to fluorite-structured $CeO_2$ (JSPDS 34-394)[32,33], indicating $CeO_2$-H and $CeO_2$-P were successfully synthesized. The crystalline structure of $CeO_2$ changed little after the loading of Ni (Fig. 1b), and no obvious diffraction peaks assigned to Ni species were observed. ICP results showed that the actual Ni loading for Ni/$CeO_2$-H (0.80 wt%), Ni/$CeO_2$-C (0.84 wt%) and Ni/$CeO_2$-P (0.81 wt%) was low, which may below the detection limit of XRD analysis.

**Textural properties of $CeO_2$ and Ni/$CeO_2$ catalysts.** The textual properties of $CeO_2$ and Ni/$CeO_2$ catalysts were obtained by $N_2$ adsorption–desorption technique, and $N_2$ adsorption–desorption isotherms of different Ni/$CeO_2$ based catalysts were shown in Fig. 2. The H4 hysteresis loops of Ni/$CeO_2$-H and Ni/$CeO_2$-P suggested the presence of mesoporous structures and the volume of mesoporous ($V_{mes}$) (Table 1) verified it. The specific surface area ($S_{BET}$) was also given in Table 1, and as can be seen that after the introduction of 0.8 wt% Ni on $CeO_2$ supports, $S_{BET}$ of all the three catalysts decreased slightly and $V_{mes}$ remained the same.

**Morphologies of Ni/$CeO_2$ catalysts.** The morphologies of Ni/$CeO_2$ catalysts were observed via TEM and SEM. Over the TEM images of three Ni/$CeO_2$ catalysts (Fig. 3), nanoparticles assigned to $CeO_2$ could be clearly

| Sample | $S_{BET}$ ($m^2\ g^{-1}$) | $V_{mes}$[a] ($cm^3\ g^{-1}$) | Crystallite size (nm) |
|---|---|---|---|
| $CeO_2$-C | 7.3 | 0.02 | 60–100 |
| $CeO_2$-P | 39. 6 | 0.11 | 10–40 |
| $CeO_2$-H | 25.7 | 0.13 | 10 |
| Ni/$CeO_2$-C | 5.4 | 0.02 | 60–100 |
| Ni/$CeO_2$-P | 35.5 | 0.11 | 10–40 |
| Ni/$CeO_2$-H | 22.4 | 0.13 | 10 |

**Table 1.** Textural properties of $CeO_2$ based catalysts. [a]$V_{mesopore}$ ($= V_{total} - V_{micropore}$), $P/P_0 = 0.99$.

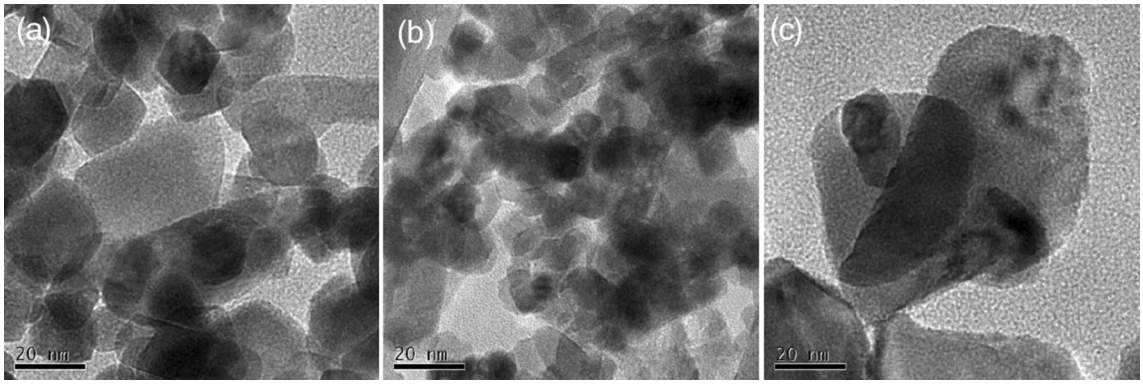


**Figure 3.** TEM images of (**a**) Ni/$CeO_2$-P, (**b**) Ni/$CeO_2$-H and (**c**) Ni/$CeO_2$-C.

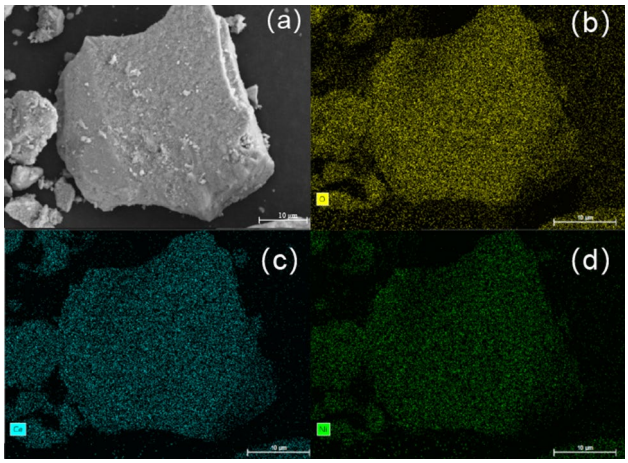


**Figure 4.** SEM image and the corresponding mapping of Ni/$CeO_2$-H catalysts: (**a**) SEM image; (**b**) O element; (**c**) Ce element; (**d**) Ni element.

observed. Obviously, $CeO_2$ over Ni/$CeO_2$-P was somewhat large, in the range of 10–40 nm (Fig. 3a); $CeO_2$ over Ni/$CeO_2$-H was relatively uniform and small, around 10 nm (Fig. 3b); Meanwhile, the size of $CeO_2$ over Ni/$CeO_2$-C was the largest, 60–100 nm (Fig. 3c). Notably, no Ni species were detected in the TEM images, inferring that Ni was well dispersed on three catalysts, and the crystallite size of $CeO_2$ in the three catalysts barely changed before and after the introduction of Ni (Table 1), which may be related to the low Ni loading.

Furthermore, the chemical analysis of the mixed oxides by SEM and the corresponding EDS were conducted to investigate the elemental distribution and the homogeneity of the three Ni/$CeO_2$ catalysts. As was shown in Fig. 4, Ni, O and Ce elements were uniformly distributed on Ni/$CeO_2$-H catalyst. The same results could also be obtained for Ni/$CeO_2$-P (Fig. S1) and Ni/$CeO_2$-C (Fig. S2), which further proved that Ni has a good dispersion state on the three Ni/$CeO_2$ catalysts.

**Acidic-basic properties of Ni/$CeO_2$ catalysts.** Acidic properties of different Ni/$CeO_2$ catalysts were characterized by $NH_3$-TPD, and the results were illustrated in Fig. 5. As was shown in Fig. 5a, there was only one obvious desorption peak (150 °C) over Ni/$CeO_2$-C corresponding to the weak acid sites. More weak (187 °C) and strong (550 °C) acid sites, especially for weak, were observed on Ni/$CeO_2$-P. It was noting that on Ni/$CeO_2$-

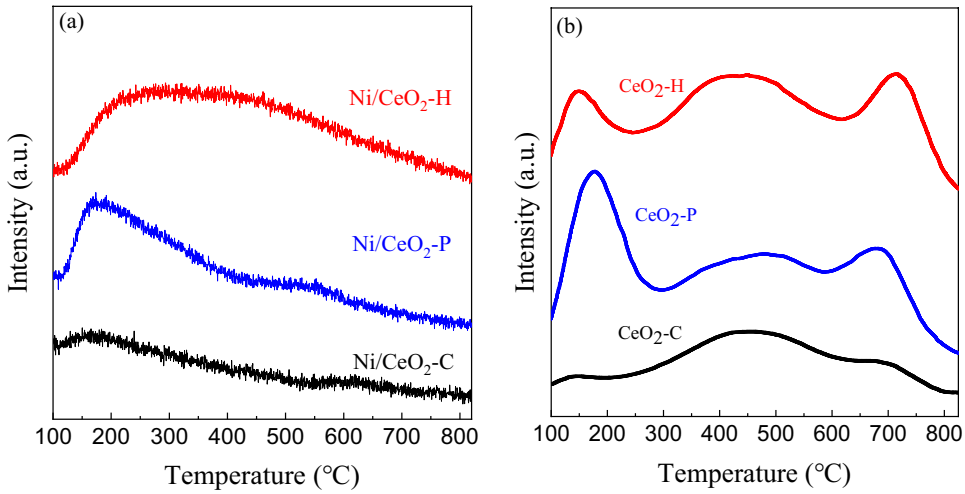


**Figure 5.** $NH_3$-TPD profiles of different (**a**) $Ni/CeO_2$ and (**b**) $CeO_2$.

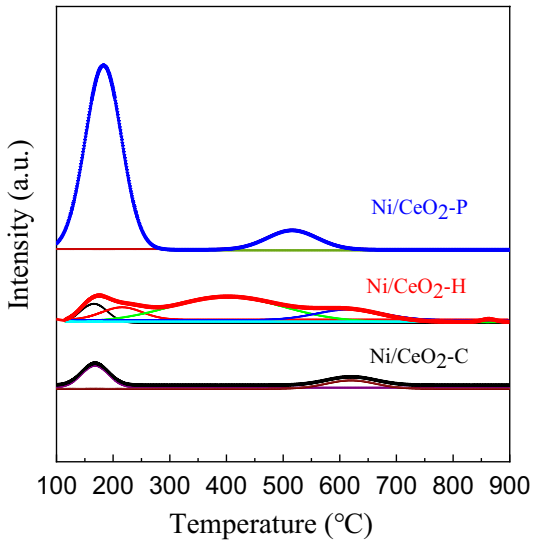


**Figure 6.** $CO_2$-TPD profiles of $Ni/CeO_2$-P, $Ni/CeO_2$-H and $Ni/CeO_2$-C.

H, there was a big and wide peak ranging from 130 to 900 °C, corresponds to the maximum amount of weak, medium and strong acid sites. The acid properties of different $CeO_2$ supports were also tested and shown in Fig. 5b. There were more weak acids on $CeO_2$-P and more medium as well as strong acid sites on $CeO_2$-H than $CeO_2$-C. Such differences came from different preparation methods of $CeO_2$.

$CO_2$-TPD experiment was performed to study the basic properties of $Ni/CeO_2$-P, $Ni/CeO_2$-H and $Ni/CeO_2$-C, and the results were shown in Fig. 6 and Table 2. It could be found that two main peaks of $CO_2$ desorption were observed at 168 °C and 620 °C over $Ni/CeO_2$-C and the overall desorption amount was the least, proving the weak and less basic sites of $Ni/CeO_2$-C. There were two peaks centered at 183 °C and 517 °C and an incredible amount of $CO_2$ desorption was detected on $Ni/CeO_2$-P, indicating a large number of weak basic sites on $Ni/CeO_2$-P. For $Ni/CeO_2$-H, there were four peaks corresponding to weak (173 °C), medium weak (402 °C), medium strong (622 °C) and strong (863 °C) basic sites, showing the diverse basic properties of the sample prepared by hydrothermal method. $CO_2$ adsorption values of prepared catalysts in Table 2 demonstrated it. It should be noted that $CO_2$ was one of the reactants, and the highest desorption temperature (863 °C) seems to mean that the binding effect between $Ni/CeO_2$-H catalyst and $CO_2$ was strong, which may be conducive to the $CO_2$ reaction.

**The state of Ni and $CeO_2$ over $Ni/CeO_2$ catalysts.** $H_2$-TPR experiment was performed to study the state of Ni and $CeO_2$ during the reducing atmosphere, and the results were shown in Fig. 7. It could be found in Fig. 7a that there were three major peaks at the temperature of 100–600 °C, 366 °C for $Ni/CeO_2$-C, 350 °C for $Ni/CeO_2$-P and 319 °C for $Ni/CeO_2$-H, respectively. It is generally accepted that the smaller the NiO particle size, the lower the hydrogen consumption temperature. Therefore, it could be inferred that the particle size of bulk

| Sample | Peak (℃) | Density (μmol$CO_2$ $g^{-1}$) |
|---|---|---|
| Ni/$CeO_2$-C | 168 | 4.3 |
| | 620 | 2.8 |
| Ni/$CeO_2$-P | 183 | 23.5 |
| | 517 | 5.6 |
| Ni/$CeO_2$-H | 173 | 4.2 |
| | 402 | 6.6 |
| | 622 | 2.4 |
| | 863 | 0.1 |

**Table 2.** $CO_2$ adsorption values for TPD experiments.

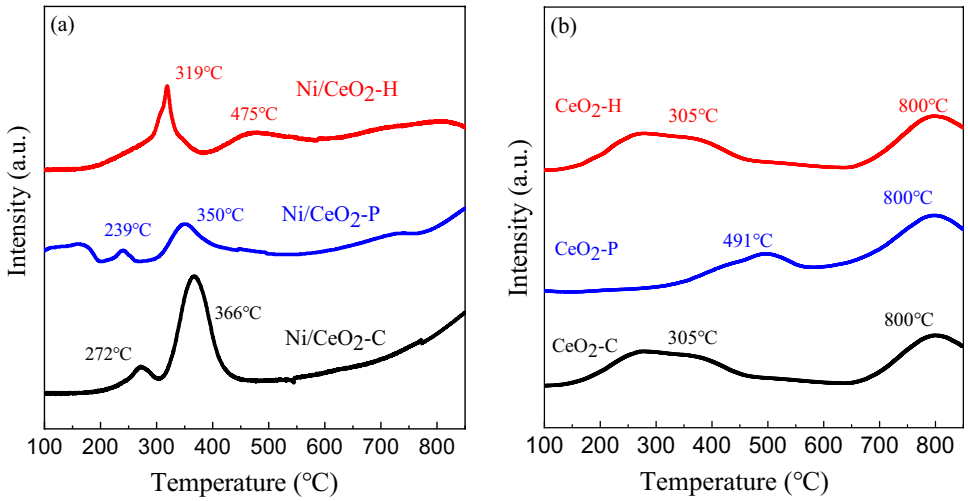


**Figure 7.** $H_2$-TPR profiles of (**a**) Ni/$CeO_2$ and (**b**) $CeO_2$.

NiO particles decreased in the order of Ni/$CeO_2$-C, Ni/$CeO_2$-P and Ni/$CeO_2$-H. There were also two relatively small peaks on Ni/$CeO_2$-P (239 °C) and Ni/$CeO_2$-C (272 °C), which were attributed to surface NiO. The $H_2$-TPR profiles of three $CeO_2$ were depicted in Fig. 7b, and as was shown that two obvious peaks could be observed on all samples: low-temperature peak for surface shell reduction ($Ce^{4+}$ to $Ce^{3+}$) and high-temperature peak for bulk reduction. Comparing the two figures in Fig. 7, the shoulder peak at 476 °C on Ni/$CeO_2$-H should be attributed to surface $CeO_2$.

**Surface structures of Ni/$CeO_2$ catalysts.** XPS was used to clarify the surface chemical environment and the valence state of elements on the reduced Ni/$CeO_2$ catalysts, and the results were shown in Fig. 8. As shown in Fig. 8a, there were three peaks located at about 853.2, 855.1, and 860.8 eV, attributed to $Ni^0$, $Ni^{2+}$, and the satellite peak of Ni $2p_{3/2}$ on reduced Ni/$CeO_2$-H[34]. In contrast, $Ni^0$ was almost absent on Ni/$CeO_2$-C and Ni/$CeO_2$-P. Figure 8b showed the XPS spectra of O 1*s* region for different Ni/$CeO_2$ catalysts. O 1*s* peaks at 528.6–529.1 eV were assigned to lattice oxygen, while peaks at 530.4–531.2 eV were assigned to oxygen vacancies. In conclusion, after reduction treatment, the most $Ni^0$ and oxygen vacancies were obtained over Ni/$CeO_2$-H among the three catalysts.

**Catalytic performance of Ni/$CeO_2$ catalysts in CRM.** The catalytic performance of Ni/$CeO_2$ catalysts in CRM were evaluated in a fixed bed reactor and the results were shown in Fig. 9. It was clear that Ni/$CeO_2$-H exhibited high catalytic activity (The initial $CO_2$ and $CH_4$ conversions were 75% and 71%, respectively). On the contrary, the catalytic performance of Ni/$CeO_2$-P and Ni/$CeO_2$-C was poor (the initial $CO_2$ and $CH_4$ conversions were within 20%). The conversion of more than five times proved the superiority of Ni/$CeO_2$-H. Due to the reverse water gas shift reaction, $CO_2$ conversion was higher than $CH_4$ conversion over all the three Ni/$CeO_2$ catalysts. After 480 min time on stream, $CO_2$ conversion dropped from 75 to 48% and $CH_4$ conversion dropped from 71 to 35%. The unsatisfied stability of Ni–$CeO_2$-H might be caused by coke. For comparison, CRM reaction of $CeO_2$-H, $CeO_2$-P and $CeO_2$-C was also evaluated. The activity of three prepared bare $CeO_2$ supports in this work was nearly inert (both $CH_4$ and $CO_2$ conversion were less than 3%), which indicated that Ni played a crucial role in CRM reaction, and the preparation method of $CeO_2$ has a great influence on the matching between Ni and $CeO_2$.

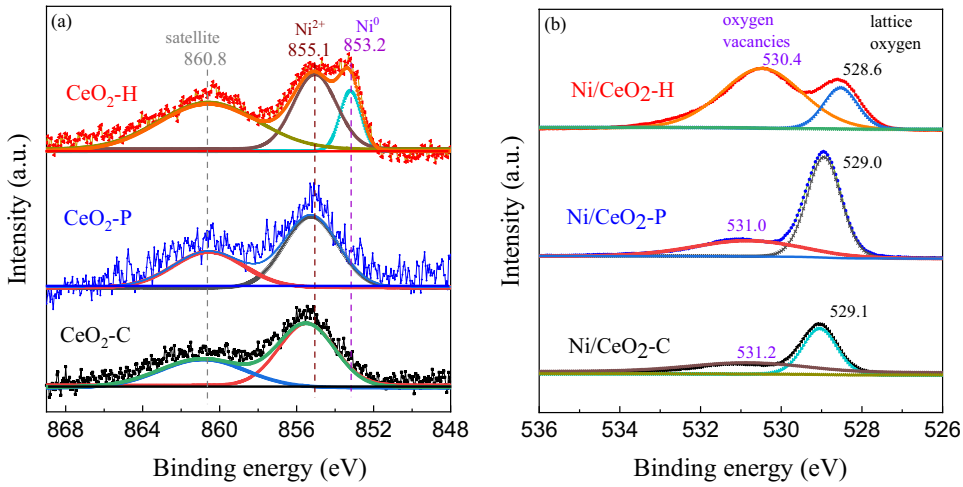


**Figure 8.** XPS spectra of (**a**) Ni $2p_{3/2}$ and (**b**) O 1*s* in the reduced Ni/$CeO_2$.

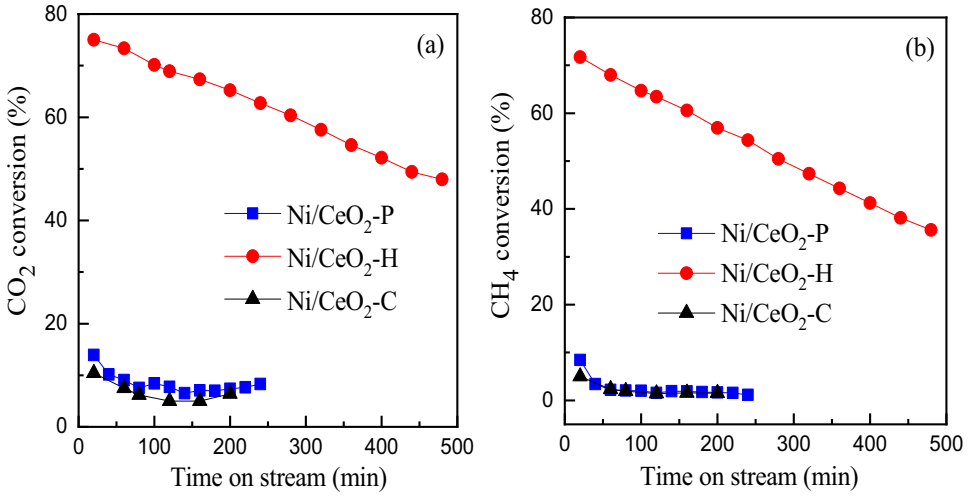


**Figure 9.** (**a**) $CO_2$ conversion and (**b**) $CH_4$ conversion of prepared Ni/$CeO_2$ catalysts as a function of time on stream. Reaction conditions: 0.20 g catalyst, $CH_4$ 20.0 mL $min^{-1}$ (STP), $CO_2$ 20.0 mL $min^{-1}$ (STP), 700 °C.

**Crystalline structure of spent Ni/$CeO_2$ catalysts.** The crystalline structure of spent Ni/$CeO_2$ catalysts was further characterized by XRD, and the results were displayed in Fig. 10. The nearly unchanged diffraction peaks between fresh and spent Ni/$CeO_2$ catalysts revealed that the crystalline structure of $CeO_2$ did not change during the reaction atmosphere. No obvious diffraction peaks assigned to Ni species were observed.

**TG of spent Ni/$CeO_2$ catalysts.** The coking behavior of spent catalysts of Ni/$CeO_2$-C, Ni/$CeO_2$-P and Ni/$CeO_2$-H was tested by TG, and the results were shown in Fig. 11. As can be seen, the similar two stages of weight change could be found over Ni/$CeO_2$-C and Ni/$CeO_2$-P, and the 0.3% increase in mass should be attributed to the oxidation process of Ni and the oxygen species adsorbed by oxygen vacancies of $CeO_2$ supports in the first stage (100–425 °C). Since the catalytic activity was weak, there was almost no weight loss for Ni/$CeO_2$-C and Ni/$CeO_2$-P in the second stage (425–850 °C). As for Ni/$CeO_2$-H, almost no weight change was observed during the first parts (100–382 °C), which may possibly because Ni and oxygen vacancies with catalytic activity were occupied by coke, and the 0.7% weight loss in the second stage (380–850 °C) should be corresponded to the amount of coke. The BET surface area of the spent Ni/$CeO_2$-H (17.9 $m^2$ $g^{-1}$) proved the covering effect of coke on the catalyst.

**Matching of Ni and $CeO_2$ on Ni/$CeO_2$ catalysts in CRM.** The activation of Ni to $CH_4$ and $CeO_2$ to $CO_2$ are very important for CRM reaction. On one hand, small Ni particles have a strong ability to activate the C-H bond of alkanes, while the aggregated Ni could easily induce $CH_4$ cracking to produce coke[12]. Therefore, it is very important to prepare small Ni particles with high dispersion. On the other hand, basic $CeO_2$ with more oxygen vacancies is beneficial to the chemisorption and dissociation of $CO_2$[35]. The results of $H_2$-TPR (Fig. 7) and XPS

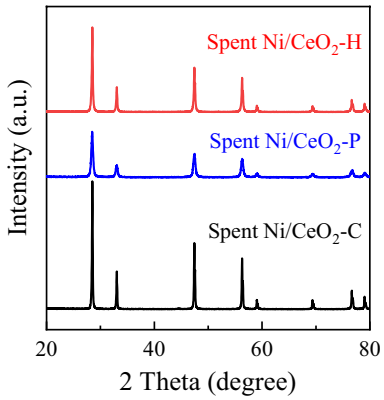


**Figure 10.** XRD patterns of spent $Ni/CeO_2$ catalysts.

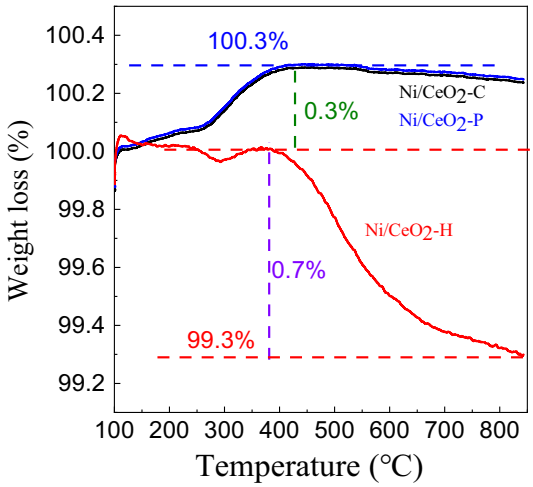


**Figure 11.** TG curves of the spent $Ni/CeO_2$-C, $Ni/CeO_2$-P and $Ni/CeO_2$-H. Reaction conditions: 0.20 g catalyst, $CH_4$ 20.0 mL $min^{-1}$ (STP), $CO_2$ 20.0 mL $min^{-1}$ (STP), 700 °C, 480 min.

(Fig. 8) manifested that small Ni and $CeO_2$ with more oxygen vacancies were obtained on $Ni/CeO_2$-H through hydrothermal method, and the matching of Ni and $CeO_2$ has been effectively demonstrated by the catalytic performance (Fig. 9). What was more, $CO_2$ dissociation and thereafter oxidation of carbon deposit can take place over low acidic catalyst system. So, Low acid catalyst system is expected to improve the stability of catalysts to a certain extent.

## Conclusions

Three $Ni/CeO_2$ catalysts were prepared by different method, and the matching between Ni and different $CeO_2$ supports as well as their effects on CRM reaction have been well studied. The conversions of $CO_2$ and $CH_4$ of $Ni/CeO_2$-P were slightly better than that of $Ni/CeO_2$-C, and the catalytic activity of $Ni/CeO_2$-H was more than 5 times that of $Ni/CeO_2$-P or $Ni/CeO_2$-C. According to the results of related characterization and evaluation, it can be concluded that the better matching of Ni and $CeO_2$, including $Ni^0$ with good dispersion and $CeO_2$ with more oxygen vacancies, was the fundamental reason for improving the reaction activity of CRM. It is a remarkable fact that coke has a great influence on the stability of catalysts, and necessary experiments are still needed. This work investigated and demonstrated the advantages and differences of hydrothermal preparation of $CeO_2$ supports and throw new light on the design of highly efficient $Ni/CeO_2$ catalysts for CRM.

Received: 31 December 2021; Accepted: 21 March 2022
Published online: 29 March 2022

## References

1. Löfberg, A., Kane, T., Guerrero-Caballero, J. & Jalowiecki-Duhamel, L. Chemical looping dry reforming of methane: Toward shale-gas and biogas valorization. *Chem. Eng. Process. Process Intens.* **122**, 523–529 (2017).

2. Martinez-Gomez, J., Nápoles-Rivera, F., Ponce-Ortega, J. M. & El-Halwagi, M. M. Optimization of the production of syngas from shale gas with economic and safety considerations. *Appl. Therm. Eng.* **110**, 678–685 (2017).
3. Fan, M.-S., Abdullah, A. Z. & Bhatia, S. Catalytic technology for carbon dioxide reforming of methane to Synthesis Gas. *ChemCatChem* **1**, 192–208 (2009).
4. Pakhare, D. & Spivey, J. A review of dry ($CO_2$) reforming of methane over noble metal catalysts. *Chem. Soc. Rev.* **43**, 7813–7837 (2014).
5. Maestri, M., Vlachos, D. G., Beretta, A., Groppi, G. & Tronconi, E. Steam and dry reforming of methane on Rh: Microkinetic analysis and hierarchy of kinetic models. *J. Catal.* **259**, 211–222 (2008).
6. Ferreira-Aparicio, P., Rodriguez-Ramos, I., Anderson, J. A. & Guerrero-Ruiz, A. Mechanistic aspects of the dry reforming of methane over ruthenium catalysts. *Appl. Catal. A* **202**, 183–196 (2000).
7. Barama, S., Dupeyrat-Batiot, C., Capron, M., Bordes-Richard, E. & Bakhti-Mohammedi, O. Catalytic properties of Rh, Ni, Pd and Ce supported on Al-pillared montmorillonites in dry reforming of methane. *Catal. Today* **141**, 385–392 (2009).
8. Abdullah, B., Ghani, N. A. A. & Vo, D.-V.N. Recent advances in dry reforming of methane over Ni-based catalysts. *J. Clean. Prod.* **162**, 170–185 (2017).
9. Wang, Y., Yao, L., Wang, S., Mao, D. & Hu, C. Low-temperature catalytic $CO_2$ dry reforming of methane on Ni-based catalysts: A review. *Fuel Process. Technol.* **169**, 199–206 (2018).
10. Zhang, G., Liu, J., Xu, Y. & Sun, Y. A review of $CH_4$-$CO_2$ reforming to synthesis gas over Ni-based catalysts in recent years (2010–2017). *Int. J. Hydrogen Energy* **43**, 15030–15054 (2018).
11. Xie, T., Shi, L., Zhang, J. & Zhang, D. Immobilizing Ni nanoparticles to mesoporous silica with size and location control via a polyol-assisted route for coking- and sintering-resistant dry reforming of methane. *Chem. Commun.* **50**, 7250–7253 (2014).
12. Therdthianwong, S., Siangchin, C. & Therdthianwong, A. Improvement of coke resistance of $Ni/Al_2O_3$ catalyst in $CH_4/CO_2$ reforming by $ZrO_2$ addition. *Fuel Process. Technol.* **89**, 160–168 (2008).
13. Das, S. *et al.* Silica-Ceria sandwiched Ni core-shell catalyst for low temperature dry reforming of biogas: Coke resistance and mechanistic insights. *Appl. Catal. B* **230**, 220–236 (2018).
14. Taherian, Z., Yousefpour, M., Tajally, M. & Khoshandam, B. Catalytic performance of Samaria-promoted Ni and Co/SBA-15 catalysts for dry reforming of methane. *Int. J. Hydrogen Energy* **42**, 24811–24822 (2017).
15. Newnham, J., Mantri, K., Amin, M. H., Tardio, J. & Bhargava, S. K. Highly stable and active Ni-mesoporous alumina catalysts for dry reforming of methane. *Int. J. Hydrogen Energy* **37**, 1454–1464 (2012).
16. Zhou, L., Li, L., Wei, N., Li, J. & Basset, J.-M. Effect of $NiAl_2O_4$ formation on $Ni/Al_2O_3$ stability during dry reforming of methane. *ChemCatChem* **7**, 2508–2516 (2015).
17. Jing, J.-Y., Wei, Z.-H., Zhang, Y.-B., Bai, H.-C. & Li, W.-Y. Carbon dioxide reforming of methane over MgO-promoted $Ni/SiO_2$ catalysts with tunable Ni particle size. *Catal. Today* **356**, 589–596 (2020).
18. Wang, F. *et al.* $CO_2$ reforming with methane over small-sized $Ni@SiO_2$ catalysts with unique features of sintering-free and low carbon. *Appl. Catal. B* **235**, 26–35 (2018).
19. García, V., Fernández, J. J., Ruíz, W., Mondragón, F. & Moreno, A. Effect of MgO addition on the basicity of $Ni/ZrO_2$ and on its catalytic activity in carbon dioxide reforming of methane. *Catal. Commun.* **11**, 240–246 (2009).
20. Osaki, T. Role of alkali or alkaline earth metals as additives to $Co/Al_2O_3$ in suppressing carbon formation during $CO_2$ reforming of $CH_4$. *Kinet. Catal.* **60**, 818–822 (2019).
21. Özcan, M. D., Özcan, O., Kibar, M. E. & Akin, A. N. Preparation of Ni-$CeO_2$/MgAl hydrotalcite-like catalyst for biogas oxidative steam reforming. *J. Fac. Eng. Arch. Gazi Univ.* **34**, 1128–1142 (2019).
22. Wang, S. & Lu, G. Q. Role of $CeO_2$ in $Ni/CeO_2$-$Al_2O_3$ catalysts for carbon dioxide reforming of methane. *Appl. Catal. B* **19**, 267–277 (1998).
23. Paunović, V., Zichittella, G., Mitchell, S., Hauert, R. & Pérez-Ramírez, J. Selective methane oxybromination over nanostructured ceria catalysts. *ACS Catal.* **8**, 291–303 (2018).
24. Machida, M., Kawada, T., Fujii, H. & Hinokuma, S. The role of $CeO_2$ as a gateway for oxygen storage over $CeO_2$-Grafted $Fe_2O_3$ composite materials. *J. Phys. Chem. C* **119**, 24932–24941 (2015).
25. Liu, C. *et al.* Synthesis of Ni-$CeO_2$ nanocatalyst by the microemulsion-gas method in a rotor-stator reactor check. *Chem. Eng. Process. Process Intens.* **130**, 93–100 (2018).
26. Yahi, N., Menad, S. & Rodríguez-Ramos, I. Dry reforming of methane over $Ni/CeO_2$ catalysts prepared by three different methods. *Green Process. Synth.* **4**, 479–486 (2015).
27. Gonzalez-Delacruz, V. M., Ternero, F., Pereñíguez, R., Caballero, A. & Holgado, J. P. Study of nanostructured $Ni/CeO_2$ catalysts prepared by combustion synthesis in dry reforming of methane. *Appl. Catal. A* **384**, 1–9 (2010).
28. Padi, S. P. *et al.* Coke-free methane dry reforming over nano-sized NiO-$CeO_2$ solid solution after exsolution. *Catal. Commun.* **138**, 105951 (2020).
29. Liu, Z. *et al.* Dry reforming of methane on a highly-active Ni-$CeO_2$ catalyst: Effects of metal-support interactions on C–H bond breaking. *Angew. Chem. Int. Ed.* **55**, 7455–7459 (2016).
30. Lustemberg, P. G. *et al.* Room-temperature activation of methane and dry re-forming with $CO_2$ on Ni-$CeO_2$ (111) surfaces: Effect of $Ce^{3+}$ sites and metal-support interactions on C–H bond sleavage. *ACS Catal.* **6**, 8184–8191 (2016).
31. Odedairo, T., Chen, J. & Zhu, Z. Metal-support interface of a novel Ni-$CeO_2$ catalyst for dry reforming of methane. *Catal. Commun.* **31**, 25–31 (2013).
32. Wang, X. *et al.* In situ studies of the active sites for the water gas shift reaction over Cu-$CeO_2$ catalysts: Complex interaction between metallic copper and oxygen vacancies of ceria. *J. Phys. Chem. B* **110**, 428–434 (2006).
33. Ho, C., Yu, J. C., Kwong, T., Mak, A. C. & Lai, S. Morphology-controllable synthesis of mesoporous $CeO_2$ nano- and microstructures. *Chem. Mater.* **17**, 4514–4522 (2005).
34. Qin, Z., Chen, L., Chen, J., Su, T. & Ji, H. Ni/CeO2 prepared by improved polyol method for CRM with highly dispersed Ni. *Greenh. Gases Sci. Technol.* **11**, 1245–1264 (2021).
35. Cárdenas-Arenas, A., Bailón-García, E., Lozano-Castelló, D., Costa, P. D. & Bueno-López, A. Stable NiO–$CeO_2$ nanoparticles with improved carbon resistance for methane dry reforming. *J. Rare Earths* **40**, 57–62 (2022).


## Acknowledgements

This work received financial support from the National Natural Science Foundation of China (21902116).

## Author contributions

Z.N.: Investigation, Data curation, Writing—original draft. X.D.: Data curation, Writing—review & editing. X.G.: Writing—review & editing. J.W.: Formal analysis. H.L.: Conceptualization, Supervision, Writing—review & editing, Funding acquisition. Q.Z.: Writing—review & editing. All authors reviewed the manuscript.

## Competing interests

The authors declare no competing interests.

## Additional information

**Supplementary Information** The online version contains supplementary material available at https://doi.org/10.1038/s41598-022-09291-w.

**Correspondence** and requests for materials should be addressed to Z.N. or H.L.

**Reprints and permissions information** is available at www.nature.com/reprints.

**Publisher's note** Springer Nature remains neutral with regard to jurisdictional claims in published maps and institutional affiliations.